

# Single-qubit unitary gates by graph scattering

Benjamin A. Blumer,<sup>\*</sup> Michael S. Underwood,<sup>\*</sup> and David L. Feder<sup>†</sup>

*Institute for Quantum Information Science, University of Calgary, Alberta T2N 1N4, Canada*

(Dated: November 17, 2011)

We consider the effects of plane-wave states scattering off finite graphs, as an approach to implementing single-qubit unitary operations within the continuous-time quantum walk framework of universal quantum computation. Four semi-infinite tails are attached at arbitrary points of a given graph, representing the input and output registers of a single qubit. For a range of momentum eigenstates, we enumerate all of the graphs with up to  $n = 9$  vertices for which the scattering implements a single-qubit gate. As  $n$  increases, the number of new unitary operations increases exponentially, and for  $n > 6$  the majority correspond to rotations about axes distributed roughly uniformly across the Bloch sphere. Rotations by both rational and irrational multiples of  $\pi$  are found.

## I. INTRODUCTION

Quantum walks are the quantum mechanical analogs of random walks in classical systems, and like their classical counterparts they have provided a useful framework for the construction of efficient quantum algorithms [1–4]. In addition to the development of quantum walk approaches to known quantum algorithms such as the Grover search [5], triangle finding [6], and element distinctness [7], several quantum algorithms were obtained using quantum walks that were previously not found within the standard quantum circuit or adversary models, such as the traversal of glued-tree graphs with randomness [8], and the solution of NAND trees [9, 10], min-max trees [11], and general boolean functions [12, 13]. More recently it has been shown that quantum walks are able to perform arbitrary quantum computational tasks [14–16].

In the continuous-time approach to universal quantum walks [14], computational basis states are represented by long linear graphs (tails) which support plane wave modes characterized by momentum eigenstates. A single quantum walker is initialized in a momentum eigenstate of a single semi-infinite line out of  $2^N$  such tails representing  $N$  qubits. Quantum operations on the encoded information are carried out by interspersing the tails with small graphs. The scattering of the plane waves off these graphs mixes the amplitudes on different tails and adds possible phase shifts.

In Ref. [14], a small number of such graphs were identified that could generate a universal set of  $N$ -qubit unitary gates for a fixed momentum  $k = -\pi/4$  (all length units are suppressed for convenience). The two graphs needed for single-qubit operations are shown in Fig. 1. The first of these, depicted in Fig. 1a, is a disconnected seven-vertex graph that yields the unitary  $R_Z(-\pi/4) = \text{diag}(1, e^{-i\pi/4}) \equiv T$  neglecting unimportant overall phases ( $R_a(\theta)$  denotes a rotation about axis  $a$  by an angle  $\theta$ , and  $X$ ,  $Y$ , and  $Z$  are the Pauli matrices). The upper subgraph is a two-site graph, so with

the tails encoding the  $|1\rangle_{\text{input}}$  and  $|1\rangle_{\text{output}}$  attached it has the effect of changing the length of the full tail by one lattice spacing. For plane waves of the form  $e^{ikx}$ , this corresponds to a scattering phase shift of  $-\pi/4$  on the  $|1\rangle$  state. The lower subgraph, attached to the  $|0\rangle$  input and output tails on the same vertex, produces no scattering phase shift and one thus obtains the desired rotation. This subgraph furthermore has the desirable property of also having an *effective length* of one lattice spacing, so that the registers  $|0\rangle$  and  $|1\rangle$  maintain their spatial coherence after the scattering event. Under this scheme the various paths through a graph be of equal length, and there must be an identity gate with the same effective length for a given momentum to act on all registers where no gate is desired. This identity requirement is trivial to satisfy in the case of graphs with integral effective lengths, but as we show below graphs can have lengths that are non-integral, or even irrational.

The second graph, shown in Fig. 1b, is a connected graph that yields  $R_X(\pi/2) \equiv V$ , again neglecting unimportant overall phases. The Hadamard gate can be constructed via  $H = T^2VT^2$ , and combinations of  $H$  and  $T$  can produce any single-qubit unitary at fixed accuracy [17]. While these two graphs are sufficient to generate a universal set of single-qubit gates, and a universal set of gates when an entangling gate is included [14], it is not clear if there are other graphs that could be chosen instead.

An immediate question is: are there other graph combinations that work equally well for  $k = -\pi/4$ , or for other values of the momentum? Because the number of non-isomorphic graphs grows exponentially in the number of vertices  $n$ , one might expect a plethora of choices which would be useful in the design of quantum algorithms based on quantum walks. Yet it is also conceivable that larger graphs will simply reproduce the unitaries found for smaller graphs, or that as  $n$  increases the requirement that there be perfect transmission from each of the input tails to the combination of the two outputs, with equal effective lengths on all four paths, will become increasingly difficult to satisfy.

In the present work, we explore these issues numerically by calculating the single-qubit unitary operators resulting from two input tails scattering to two output

<sup>\*</sup> These authors contributed equally to this work.

<sup>†</sup> Corresponding author: dfeder@ucalgary.ca

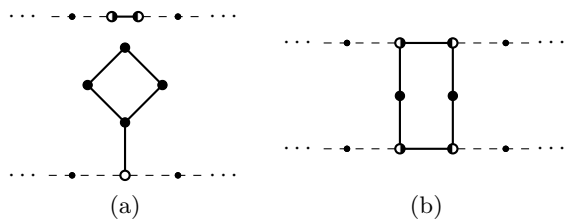


FIG. 1. The graphs identified in Ref. [14] that generate a universal set of one-qubit unitary gates, with vertices denoted by circles and edges by solid lines. Open circles indicate that both an input and an output tail attach at that vertex, whereas circles open only to the left or right indicate attachment of only input or output tails, respectively. Graphs (a) and (b) generate the rotations  $R_Z(\pi/4)$  and  $R_X(\pi/2)$ , respectively, for  $k = -\pi/4$ . The tails, depicted by dashed edges and ellipses to denote their continuation, are included to indicate the attachment vertices. These graphs appear in the supplemental material as IDs 238 and 309.

tails, off every possible graph with up to nine vertices. Momentum eigenstates  $k = (p/q)\pi$  where  $q \in \{2, 3, 4, 5\}$  and  $0 < p < q$  for integer  $p$  are considered; we study only positive values of  $k$  for two reasons. Mathematically there is a symmetry between positive and negative momenta such that negating  $k$  conjugates the reflection and transmission coefficients; physically if one considers propagating wavepackets with tightly peaked momenta instead of un-normalizable plane waves, the negative momenta result in the initial state traveling away from the scattering graph instead of toward it, under the definitions we use. Note that in Ref. [14] the graphs of Fig. 1 are utilized at momentum  $k = -\pi/4$  because the Hamiltonian employed therein is equal to the adjacency matrix of the graph, rather than its negative. We find that the number of graphs meeting the requirements for implementing single-qubit rotations does indeed grow exponentially with  $n$ . The most prolific momentum we investigate is  $k = 2\pi/3$ , which results in a total of 98 unique unitary operations on graphs of nine or fewer vertices.

There is a supplemental data file associated with this manuscript, available on the arXiv pre-print server [18], and our main focus here is the analysis of those data. This manuscript is organized as follows. The mathematical formalism underlying the scattering of plane waves by graphs is briefly reviewed in Sec. II, followed by a description of the numerical strategy to enumerate graphs. The results of the survey are given in Sec. III, and are summarized in Sec. IV.

## II. FORMALISM

### A. Graph Scattering

The theory underpinning the scattering of plane waves by graphs has been discussed in detail by Varbanov and

Brun [19], so it will only be sketched here. One considers a finite graph  $G = \{E, V\}$  with  $V$  a set of  $n$  vertices and  $E \subseteq V \times V$  a set of edges defined by the graph adjacency matrix  $A^G$ . Each vertex  $v \in V$  has attached to it  $M_v$  semi-infinite tails ( $M_v$  may vanish for as many as  $n - 1$  of the vertices of  $G$ ), with the adjacency matrix of tail  $m$  on vertex  $v$  defined as  $[A_{vm}^T]_{ij} = \delta_{i,j+1} + \delta_{i+1,j}$  where  $i, j \in \{1, 2, 3, \dots\}$ . Vertices on the tails are denoted  $|j_{vm}\rangle$ , with the attachment vertex on the graph labeled  $|0_{vm}\rangle$  where the index  $m$  is kept only to match the tail labeling, i.e.  $|0_{vm}\rangle \equiv |v\rangle$ . The adjacency matrix associated with the connection of the tails to the graph is  $A_{vm}^C = |0_{vm}\rangle\langle 1_{vm}| + |1_{vm}\rangle\langle 0_{vm}|$ , and the total adjacency matrix for the scattering system as a whole is

$$A = A^G + \sum_{v \in V} \sum_{m=1}^{M_v} (A_{vm}^T + A_{vm}^C). \quad (1)$$

To describe single-qubit unitary transformations we are interested only in those cases with four tails — two input and two output — attached to  $G$ . That is, we require

$$\sum_{v \in G} M_v = 4. \quad (2)$$

For the moment though, suppose that the graph  $G$  consists of a single point. In this case, two semi-infinite tails corresponding to the input and output states fuse into a single infinite line. The (unnormalized) eigenstates of the graph Hamiltonian  $H \equiv -A$  are plane waves

$$|k\rangle = |0\rangle + \sum_{j=1}^{\infty} (e^{-ikj}|j_{00}\rangle + e^{ikj}|j_{01}\rangle) \quad (3)$$

with eigenvalue  $\epsilon_k = -2\cos(k)$ , where  $k \in [-\pi, \pi]$  is the momentum quantum number. One can envisage the input as a wavepacket strongly peaked at momentum  $k$  scattering off a single point, resulting in an identical output wavepacket.

Now consider an arbitrary number of tails connected to an arbitrary finite graph  $G$ , again defined by adjacency matrix  $A$  and corresponding Hamiltonian  $H = -A$ . One again assumes that the input and output states are plane-wave eigenstates of their respective semi-infinite lines, with eigenvalue  $2\cos(k)$ ; that is, the scattering has not changed the value of  $k$ , equivalent to the conservation of momentum and energy. In principle the graph could mix momenta on different input and output tails; this possibility is not included in the analysis, because it would imply that the quantum information encoded in the wavepackets would travel down the tail at different rates.

Consider a momentum eigenstate  $|k, vm\rangle$  with incoming component only on tail  $m$  of vertex  $v$ , and possible outgoing components on every attached tail including the incoming one. This leads to transmission and reflection coefficients,  $t_{v'm',vm}$  and  $r_{vm}$  respectively, defined by the

expressions

$$\langle j_{vm} | k, vm \rangle = e^{-ikj} + r_{vm}(k) e^{ikj}, \quad (4)$$

$$\langle j_{v'm'} | k, vm \rangle = t_{v'm',vm}(k) e^{ikj}. \quad (5)$$

The first and second terms in Eq. (4) represent the incoming and reflected component of the state respectively. The term on the right hand side of Eq. (5) represents the component of the incoming state that is transmitted to the other tails (for which  $v' \neq v$  or  $m' \neq m$ ). These are Eqs. (4) and (5) of Varbanov and Brun [19].

The momentum eigenstates  $|k, vm\rangle$  can be expressed in terms of their components on the graph vertices  $|k, vm\rangle^G$  and the tails:

$$\begin{aligned} |k, vm\rangle &= |k, vm\rangle^G + \sum_{j=1}^{\infty} (e^{-ikj} + r_{vm} e^{ikj}) |j_{vm}\rangle \\ &+ \sum_{v',m'}' t_{v'm',vm} \sum_{j=1}^{\infty} e^{ikj} |j_{v'm'}\rangle, \end{aligned} \quad (6)$$

where the prime on the second sum indicates that all possible values of  $v'$  and  $m'$  for which  $v' \neq v$  or  $m' \neq m$  are being summed over. Enforcing the condition that  $H|k, vm\rangle = -2\cos(k)|k, vm\rangle$  and simplifying, one obtains that  $|k, vm\rangle^G$  must satisfy

$$\begin{aligned} \left( A^G - 2\cos(k) + e^{ik} \sum_{v'} M_{v'} |v'\rangle \langle v'| \right) |k, vm\rangle^G \\ = 2i \sin(k) |v\rangle. \end{aligned} \quad (7)$$

This is Eq. (10) of Varbanov and Brun [19]. The solution to the scattering problem consists of determining the vector  $|k, vm\rangle^G$  and from it obtaining the reflection and transmission coefficients. Because the reflection and transmission coefficients at the attachment points must be the same as on the tails, Eqs. (4) and (5) can be expressed more conveniently in terms of  $|k, vm\rangle^G$  and the graph vertex states as

$$\langle v | k, vm \rangle^G = 1 + r_{vm}, \quad (8)$$

$$\langle v' | k, vm \rangle^G = t_{v'm',vm}. \quad (9)$$

In order to interpret the scattering event as implementing a single-qubit operation, one assumes that the finite graph  $G$  has four semi-infinite tails attached. Two of the tails are considered as inputs and two as outputs. A continuous-time quantum walker in a wavepacket state with momentum tightly peaked about  $k$  propagates toward  $G$  along the two input tails. It scatters from an initial superposition supported on these tails to a superposition with support on the two output tails. Any relative phase shift or change in probability amplitude between the two tails corresponds to a unitary transformation of the input computational state. In general, a momentum eigenstate incoming on the first input,  $vm = 0_{\text{in}}$ , can be thought of as mapping incoming to outgoing states

according to

$$\begin{aligned} |k, 0_{\text{in}}\rangle &\mapsto r_{0_{\text{in}}}(k) |k, 0_{\text{in}}\rangle + t_{1_{\text{in}},0_{\text{in}}}(k) |k, 1_{\text{in}}\rangle \\ &+ \sum_{i=0}^1 t_{i_{\text{out}},0_{\text{in}}}(k) |k, i_{\text{out}}\rangle. \end{aligned} \quad (10a)$$

Similarly, a momentum state with incoming component on the second input,  $vm = 1_{\text{in}}$ , scatters to outgoing components as

$$\begin{aligned} |k, 1_{\text{in}}\rangle &\mapsto r_{1_{\text{in}}}(k) |k, 1_{\text{in}}\rangle + t_{0_{\text{in}},1_{\text{in}}}(k) |k, 0_{\text{in}}\rangle \\ &+ \sum_{i=0}^1 t_{i_{\text{out}},1_{\text{in}}}(k) |k, i_{\text{out}}\rangle, \end{aligned} \quad (10b)$$

so in order for these scattering processes to correspond to a unitary operation mapping  $|k, 0_{\text{in}}\rangle$  and  $|k, 1_{\text{in}}\rangle$  to superpositions of  $|k, 0_{\text{out}}\rangle$  and  $|k, 1_{\text{out}}\rangle$  we must identify combinations of graphs  $G$ ; tail attachment points  $|0_{\text{in}}\rangle$ ,  $|1_{\text{in}}\rangle$ ,  $|0_{\text{out}}\rangle$ , and  $|1_{\text{out}}\rangle$ ; and momenta  $k$  such that there is neither reflection along either input tail nor transmission from one input tail to the other. That is, we require

$$r_{0_{\text{in}}} = r_{1_{\text{in}}} = t_{0_{\text{in}},1_{\text{in}}} = t_{1_{\text{in}},0_{\text{in}}} = 0. \quad (11)$$

When the conditions Eq. (11) are met, the transformations Eq. (10) simplify to

$$|k, 0_{\text{in}}\rangle \mapsto t_{0_{\text{out}},0_{\text{in}}}(k) |k, 0_{\text{out}}\rangle + t_{1_{\text{out}},0_{\text{in}}}(k) |k, 1_{\text{out}}\rangle, \quad (12a)$$

$$|k, 1_{\text{in}}\rangle \mapsto t_{0_{\text{out}},1_{\text{in}}}(k) |k, 0_{\text{out}}\rangle + t_{1_{\text{out}},1_{\text{in}}}(k) |k, 1_{\text{out}}\rangle, \quad (12b)$$

i.e. an arbitrary input vector  $\alpha|k, 0_{\text{in}}\rangle + \beta|k, 1_{\text{in}}\rangle$  is transformed by the operator:

$$\hat{O} = \begin{pmatrix} t_{0_{\text{out}},0_{\text{in}}} & t_{0_{\text{out}},1_{\text{in}}} \\ t_{1_{\text{out}},0_{\text{in}}} & t_{1_{\text{out}},1_{\text{in}}} \end{pmatrix}. \quad (13)$$

We must now show that this operator is unitary. To simplify notation, let us label the two input tails by 1 and 2, and the output tails by 3 and 4. A general scattering process on a graph with four attached tails yields an S-matrix

$$S = \sum_{i=1}^4 \left( r_i |\tau_i\rangle \langle \tau_i| + \sum_{\substack{j=1 \\ j \neq i}}^4 t_{ij} |\tau_i\rangle \langle \tau_j| \right), \quad (14)$$

where  $|\tau_i\rangle$  corresponds to the state on tail  $i$ , which Varbanov and Brun show is unitary [19]. Our restriction that we consider only graphs satisfying Eq. (11) does not change the unitarity of  $S$  in those cases, and corresponds to  $r_1 = r_2 = t_{12} = t_{21} = 0$ . We then assume an initial state with support only on the input tails,  $|\psi_0\rangle = \alpha|\tau_1\rangle + \beta|\tau_2\rangle$ , with  $|\alpha|^2 + |\beta|^2 = 1$ . The restricted S-matrix acts on such a state as

$$S|\psi_0\rangle = (\alpha t_{31} + \beta t_{32}) |\tau_3\rangle + (\alpha t_{41} + \beta t_{42}) |\tau_4\rangle, \quad (15)$$

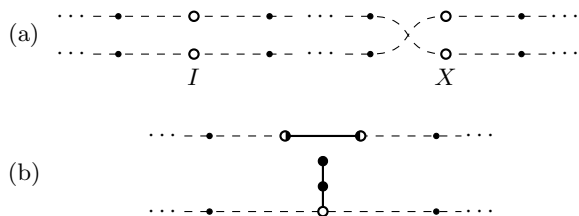


FIG. 2. (a) Given two isolated vertices off of which to scatter, the identity and SWAP gates,  $I$  and  $X$ , are trivial to construct at any momentum (supplemental material IDs 180 and 179, respectively, at  $k = \pi/4$ ). (b) With five vertices it becomes possible to implement gates other than  $I$  and  $X$ . This five-vertex graph implements  $R_Z(-\pi/2)$  and has an effective length of 1. (Supplemental material ID 1458,  $k = \pi/2$ .)

but this is precisely the action of  $\hat{O}$  on  $\alpha|k, 0_{\text{in}}\rangle + \beta|k, 1_{\text{in}}\rangle$  under the identification  $|\tau_i\rangle \leftrightarrow |k, i\rangle$  with  $1 \leftrightarrow 0_{\text{in}}$ ,  $2 \leftrightarrow 1_{\text{in}}$ ,  $3 \leftrightarrow 0_{\text{out}}$ , and  $4 \leftrightarrow 1_{\text{out}}$ . Since  $S$  is unitary in general, it remains so when restricted to the cases of interest that define  $\hat{O}$ .

### B. Enumeration of Graphs

The number of non-isomorphic simple graphs on  $n$  vertices grows super-exponentially with  $n$ , and for each graph the number of ways to attach four tails goes as  $n^4$ . Using the **geng** (*generate graphs*) software package, part of the popular **nauty** (*no automorphisms, yes?*) suite of graph theoretic tools [20], we first generate the adjacency matrices  $A^G$  of all non-isomorphic simple graphs on  $n$  vertices for  $n \in \{1, 2, 3, \dots, 9\}$ . For each graph we then enumerate the set of all combinations of attachment points for four tails, each of which defines a set  $\{M_1, M_2, \dots, M_n\}$  satisfying Eq. (2).

One can see by symmetry arguments that the one-vertex graph with four tails attached cannot transmit from one of the tails to only two of the remaining three, so at least two vertices are required to implement a computational unitary gate. With two or more vertices available, it is trivial to implement the identity gate and the SWAP or  $X$  gate by constructing a graph with two isolated vertices and attaching an input and an output tail to each one, as exemplified in Fig. 2a. If the computational labels (i.e.  $|0\rangle$  and  $|1\rangle$ ) agree on each vertex then an identity is performed; otherwise the  $X$  gate is applied. The first unitaries that cannot be trivially produced in this manner appear when there are five vertices. An example of such a graph can be found in Fig. 2b.

For each momentum value  $k$  under consideration, for each adjacency matrix  $A^G$  and attachment set  $\{M_v\}$ , Eq. (7) produces a set of  $n$  linear equations to be solved for the coefficients of  $|k, vm\rangle^G$ . These in turn yield the reflection and transmission coefficients from Eqs. (8) and (9). Due to the large number of such combinations of

$k$ ,  $\{M_v\}$ , and  $A^G$  (of order  $10^9$  under the chosen constraints), we solve these equations numerically using the GNU Scientific Library [21] and LAPACK [22] software libraries. If a particular combination results in reflection and transmission coefficients satisfying Eq. (11) then there is zero transmission from the input tail to one of the three possible output tails. In this case, we solve the equations again with the incoming portion of the momentum eigenstate instead on this unused tail. If the conditions (11) are again satisfied, with the same two tails supporting the output, then the current combination implements a unitary transformation  $U$  defined by the operator (13).

The final step is to determine the effective length through the graph from each input to each output. If paths of different length exist, then a quantum walker initially in a superposition of one wavepacket on either input tail would acquire a spatial shift between the two output wavepackets after traversing the graph. The effective length to output  $j$  from input  $i$  is defined as [14]

$$\ell_{ji}(k) = \frac{d}{dk} \arg t_{j_{\text{out}}, i_{\text{in}}}(k). \quad (16)$$

This can be understood when one considers the case of a single input attached to one end of a linear graph of  $L$  segments, with a single output tail at the other end. Clearly the transmission from one end to the other has unit magnitude at all momenta, and the phase difference between the ends results in a transmission coefficient of  $t(k) = e^{ikL}$ . Equation (16) then yields  $\ell(k) = L$ , as expected. We calculate this derivative numerically on each candidate graph, using a nine-point stencil, and require that the four values  $\ell_{ji}(k)$  agree whenever  $t_{j_{\text{out}}, i_{\text{in}}} \neq 0$ .

Our goal is to determine any potential computational advantage to increasing the number of vertices in  $G$ , so we record the current system only if  $U$  meets all of the stated criteria and has not been found at the same momentum and effective length on a smaller graph. If it has been previously found, we keep track of how many times it has appeared.

### III. RESULTS

The number of non-isomorphic simple graphs on  $n$  vertices,  $N_n$ , does not have a simple closed-form solution. Nevertheless, the counts are well documented for many values of  $n$  (see, for example, Ref. [23] and references therein), and the total number of such graphs on nine or fewer vertices is 288 266. For each graph on  $n$  vertices, the number of distinct ways to attach  $k$  tails is

$$w_n = \binom{n+k-1}{k}, \quad (17)$$

and we have chosen to investigate scattering at nine different momenta with four attached tails. This results

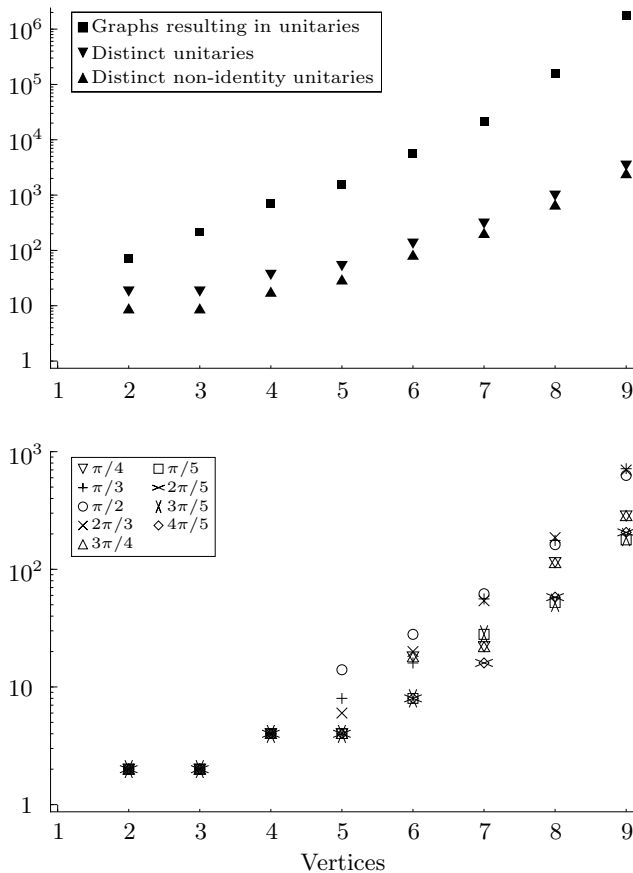


FIG. 3. (Top) Total number of graphs resulting in unitary operators, as well as the number of distinct unitaries found as a function of number of vertices. Here operations are considered distinct if they arise from graphs with different effective lengths or at different momenta. (Bottom) Number of distinct unitaries, as presented in the upper plot, separated by momentum.

in

$$9 \sum_{n=1}^9 N_n w_n = 1\,262\,489\,148 \quad (18)$$

combinations of momenta, attachment points, and graphs to be numerically examined. Of these, it turns out that 1960316 have the properties required to implement a computational gate. Figure 3 shows that the number of unitary and non-identity operations both increase super-exponentially in the number of vertices, following the growth of the total number of graphs, and that this is true at each momentum investigated.

There is significant redundancy within these gates however, where many different graphs yield the same unitary for a given value of the momentum and effective length. This reduces the total number of distinct unitary operations to 3380. The adjacency matrices for these graphs, the relevant momentum and attachment points, and the resulting unitary gates arising, are given

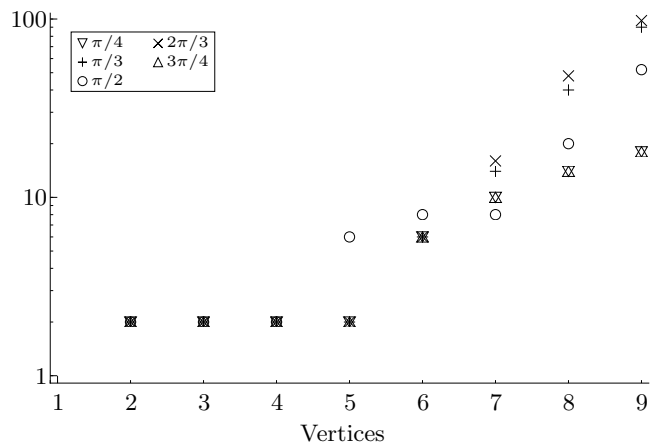


FIG. 4. Number of available unitaries provided by increasing the number of vertices in the scattering graph, for the five  $k$  values at which an increase was found. Here we do not consider unitaries to be distinct if they arise at different effective lengths but otherwise perform the same transformation.

explicitly in the supplemental online information accompanying this work [18]. Of the graphs producing these, 2496 yield gates other than identities; that said, it is important to keep in mind that an identity counterpart is required for each non-identity gate in order to ensure universality so having a sufficiently large number of identity gates is essential.

Only those graphs which result in unitary operations at the same momentum value can be combined under the current model to effect a quantum computation, since the momentum of the quantum walker is fixed. The effective lengths of the constituent graphs are unimportant, as long as each graph can be paired with an identity operation of the same length. There are 262 graphs which do not have commensurate identity graphs, leaving 3118 candidates for inclusion in computational sets. There is further redundancy among these graphs, since two graphs performing the same operation with different effective lengths at the same momentum are for our purposes equivalent if each has a corresponding identity operation. Taking this into account reduces the number of potentially useful operations to 284. The number of resulting unitaries is shown in Fig. 4 as a function of the number of vertices for the momentum values investigated. There are 16 unitaries that can be produced by graphs on five vertices, eight of which are new in that they cannot be produced by four or fewer vertices. Similarly, there are 24 new unitaries on six vertices, and 30 more on seven. These 62 unitary operators are produced by only 15 graphs, combined with various tail attachment and momentum configurations. One of these graphs has two variations of tail attachment points that lead to non-isomorphic infinite graphs once the tails are included. These 16 graphs are drawn explicitly in Fig. 5.

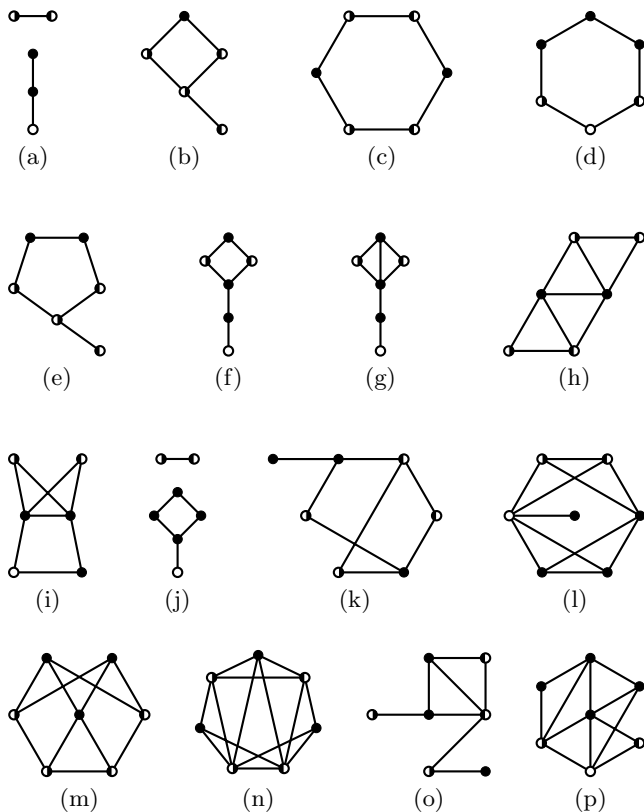


FIG. 5. The graphs on five, six, or seven vertices that implement single-qubit unitaries which are unavailable on fewer vertices. The five-vertex graphs (a) and (b) result in eight distinct unitaries under different tail attachment configurations and different momentum values. The six-vertex graphs (c)-(i) yield a total of 24 unitaries, and the seven-vertex graphs (j)-(p) lead to 30. Note that while (c) and (d) are isomorphic, they represent two distinct, non-isomorphic configurations once tails are attached.

### A. Unitary operations by momentum value

There are four momentum values,  $p\pi/5$  for  $p = 1, 2, 3, 4$ , at which the only available operations are the identity and Pauli- $X$  operators; these momenta are clearly not useful for our purposes, and are therefore not plotted. It is clear that for each momentum value that provides a growing number of unitaries, the number of unique gates continues the exponentially increasing trend as a function of the number of vertices.

At  $k = \pi/4$  we find graphs that implement Pauli- $X$ ,  $-Y$ , and  $-Z$  gates as well as the rotations  $R_X(\pm\pi/2)$  and  $R_Z(p\pi/4)$  for  $p \in \{-3, -2, \dots, 3\}$  (the latter including the identity at  $p = 0$ ). These results contain the graphs identified by Childs [14] and therefore (re)produce a universal set of gates. Additionally, we find graphs producing rotations by  $-\pi$  about those axes in the equatorial plane of the Bloch sphere making angles with respect to the  $X$  axis of  $p\pi/8$  for  $p \in \{1, 2, 3, 5, 6, 7\}$ . Momentum

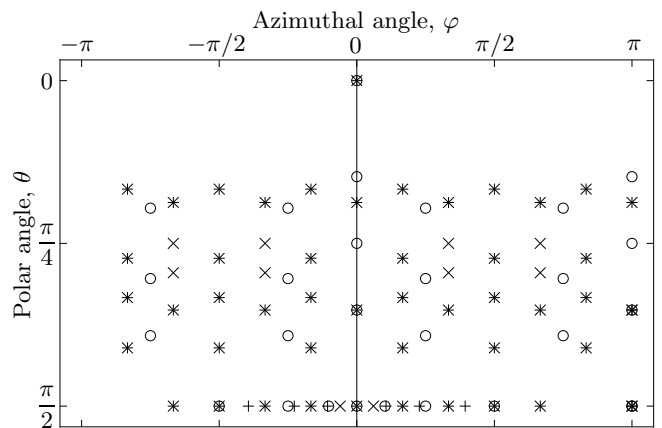


FIG. 6. Distributions of the axes of rotation on the Bloch sphere available at momentum values  $k = \pi/2, \pi/3$ , and  $2\pi/3$ . That is, there exists at least one non-trivial rotation  $R_{(\theta, \varphi)}$  about each axis defined by the points  $(\theta, \varphi)$  on the upper hemisphere of the Bloch sphere shown here. Symbols are as in Fig. 4.

$k = 3\pi/4$  reproduces this same set of 18 gates.

When the momentum is  $k = \pi/2$  we find graphs capable of implementing 52 rotations of the Bloch sphere, about 28 non-parallel axes. With momenta  $k = \pi/3$  and  $k = 2\pi/3$  we find 90 and 98 rotations about 55 and 59 distinct axes, respectively. The available axes are visualized for these three momentum values in Fig. 6. The reflection symmetries about  $\phi = 0$  and  $\phi = \pm\pi/2$  are due to the different configurations of attachment points available for each graph. If a given graph performs a single-qubit rotation about the  $(\theta, \phi)$  axis of the Bloch sphere when the attachment vertices for  $(|0\rangle_{\text{in}}, |1\rangle_{\text{in}}, |0\rangle_{\text{out}}, |1\rangle_{\text{out}})$  are  $(|1\rangle, |2\rangle, |3\rangle, |4\rangle)$ , then moving the inputs to the outputs and vice versa by re-attaching the tails in the order  $(|3\rangle, |4\rangle, |1\rangle, |2\rangle)$  results in a rotation about  $(\theta, -\phi)$ . Interchanging the inputs with each other and doing the same for the outputs, i.e. re-ordering the tails as  $(|2\rangle, |1\rangle, |4\rangle, |3\rangle)$ , leads to a rotation about  $(\theta, \pi - \phi)$ . This re-ordering is equivalent to conjugating the original gate by  $X$ .

### B. Rotations by irrational multiples of $\pi$ ; fractional and irrational effective lengths.

Figure 7 showcases three graphs that produce interesting and perhaps unexpected results. While there is no reason to assume *a priori* that our procedure will not find any rotations by irrational multiples of  $\pi$ , neither is it intuitive that this should be the case given that the graphs are scattering plane waves with momentum values that are rational fractions of  $\pi$ . Nevertheless, we indeed identify over 100 rotations through angles that numerically appear to be irrational fractions of  $\pi$ . These individual

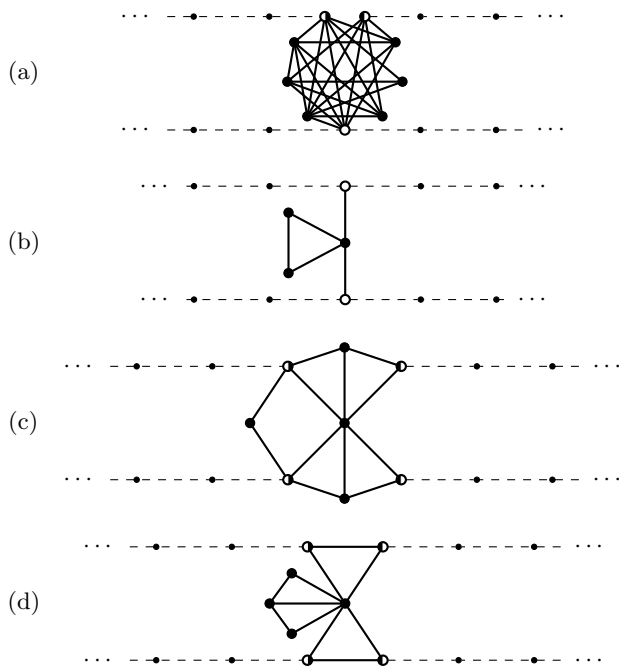


FIG. 7. Some graphs that exhibit non-intuitive properties. At  $k = \pi/3$ , (a) performs a  $Z$  rotation through an angle of  $\arctan(5\sqrt{3}/11)$ , followed by a  $Z$  gate. Also at  $k = \pi/3$ , (b) is an identity gate with an effective length of  $\ell = 1/2$ . Finally at  $k = \pi/4$ , (c) performs the basis-changing operation  $\sqrt{X}$  and (d) implements an identity, each with the irrational effective length of  $\ell = 5 - 2\sqrt{2}$ . (Supplemental material IDs 802, 488, 327, and 330.)

results can be checked analytically by solving Eqs. (7)-(9) exactly in the cases of interest; those we checked bore out the apparent irrationality indicated by the numerical results. Figure 7a depicts one such case, a graph that implements the transformation  $ZR_Z[\arctan(5\sqrt{3}/11)]$  up to a global phase at momentum  $k = \pi/3$ . Besides the novelty of obtaining irrational multiples of  $\pi$  under the circumstances, these graphs are inherently useful because any two rotations about non-parallel axes by irrational multiples of  $\pi$  form a universal set for fixed-precision single-qubit quantum computation [17].

Similarly, it is not obvious whether any graph should have a non-integral effective length. Figure 7b shows a graph on only five vertices that is capable of acting as an identity gate with an effective length of  $\ell = 1/2$ ; at the momenta in question, no graph exists on fewer than five vertices that has a non-integral effective length and implements a single-qubit unitary. Finally we see in Fig. 7c a graph that has an irrational effective length of  $\ell = 5 - 2\sqrt{2}$ . This graph implements the basis-changing operation  $\sqrt{X}$ , and remarkably the graph in Fig. 7d acts as an identity gate with this same irrational length. Of the 3118 graphs capable of implementing single-qubit unitaries with commensurate identities, 2352 of them

have non-integral effective lengths. Of these, 1042 appear numerically to have irrational lengths, including the ‘longest’ graph identified, which has effective length  $\ell = 350 + 156\sqrt{5} \approx 698.826$  (ID 2174 in supplemental material [18]). This extreme effective length due to a comparatively small number of vertices (i.e.  $9 \ll 700$ ) is another observed phenomenon whose presence is not initially obvious. Such a length corresponds to the incoming wavepacket’s having been localized in the region of the graph for a significant duration, and is reminiscent of a diverging negative scattering length, approaching unitarity in traditional quantum scattering theory. Almost 20% of the unitaries identified have effective lengths  $\ell \geq 10$ , with greater than 1% having  $\ell \geq 100$ . In the same vein, it is also noteworthy that no negative effective lengths were identified.

#### IV. CONCLUSIONS

Inspired by the proof due to Childs that wavepackets scattering off small simple graphs can perform universal quantum computation, we have exhaustively studied scattering at nine momenta over the set of graphs on fewer than 10 vertices. As the number of vertices in the scattering center increases, so does the number of distinct single-qubit unitary operations that can be performed. The number of distinct graphs capable of producing these unitaries grows super-exponentially, providing many methods by which to construct a given operator. The promise of investigating graphs on larger number of vertices is that a desired operation might be able to be implemented by scattering off one or a few graphs, where its decomposition into the two transformations in a single universal set could require many more.

Rotations of the Bloch sphere can be performed about many axes distributed roughly uniformly across its surface, by both rational and irrational multiples of  $\pi$ . This results in a large number of distinct sets of operators that are universal for quantum computation, which can be combined together to minimize the total size of the graph used in a computation. Natural extensions to this work include increasing the number of vertices under investigation, the array of momenta studied, or both; and expanding the number of tails attached to each scattering graph to find two- or three-qubit gates (or more).

#### ACKNOWLEDGMENTS

We are grateful to Andrew Childs for helpful comments in the early stages of this work. The authors acknowledge funding from Alberta Innovates – Technology Futures (MSU), and the Natural Sciences and Engineering Research Council of Canada.

- 
- [1] A. Ambainis, *Int. J. Quant. Inf.* **1**, 507 (2003).
- [2] J. Kempe, *Contemporary Physics* **44**, 307 (2003).
- [3] V. Kendon, *Math. Struct. Comp. Sci.* **17**, 1169 (2007).
- [4] V. Kendon, e-print: [arXiv:1107.3795](https://arxiv.org/abs/1107.3795) (2011).
- [5] M. Santha, in *Theory and Applications of Models of Computation* (Springer Berlin / Heidelberg, 2008), vol. 4978, pp. 31-46.
- [6] F. Magniez, M. Santha, and M. Szegedy, Proceedings of the sixteenth annual ACM-SIAM symposium on Discrete algorithms (SODA 2005), p. 1109 (2005).
- [7] A. Ambainis, *SIAM Journal on Computing* **37**, 210 (2007).
- [8] A. M. Childs, R. Cleve, E. Deotto, E. Farhi, S. Gutmann, and D. A. Spielman, Proceedings of the 35th ACM Symposium on Theory of Computing (STOC 2003), p. 59 (2003).
- [9] E. Farhi, J. Goldstone, S. Gutmann, *Theory of Computing* **4**, 169 (2008).
- [10] A. M. Childs, R. Cleve, S. P. Jordan, and D. Yeung, *Theory of Computing* **5**, 119 (2009).
- [11] R. Cleve, D. Gavinsky, and D. L. Yonge-Mallo, in *Theory of Quantum Computation, Communication, and Cryptography* (Springer-Verlag Berlin, Heidelberg, 2008).
- [12] B. W. Reichardt and R. Spalek, Proceedings of the 40th ACM Symposium on Theory of Computing (STOC 2008), p. 103 (2008).
- [13] A. Ambainis, A. M. Childs, B. W. Reichardt, R. Spalek, and S. Zhang, *SIAM J. Comput.* **39**, 2513 (2010).
- [14] A. M. Childs, *Phys. Rev. Lett.* **102**, 180501 (2009).
- [15] N. B. Lovett, S. Cooper, M. Everitt, M. Trevers, and V. Kendon, *Phys. Rev. A* **81**, 042330 (2010).
- [16] M. S. Underwood and D. L. Feder, *Phys. Rev. A* **82**, 042304 (2010).
- [17] P. Kaye, R. Laflamme, and M. Mosca, *An Introduction to Quantum Computation*, pp. 70-71 (Oxford University Press, 2007).
- [18] See Supplemental Material included with this manuscript at <http://www.arxiv.org> for a complete list of unitary gates found.
- [19] M. Varbanov and T. A. Brun, *Phys. Rev. A* **80**, 52330 (2009).
- [20] B. D. McKay, <http://cs.anu.edu.au/~bdm/nauty>.
- [21] M. Galassi et al., *GNU Scientific Library Reference Manual*, <http://www.gnu.org/software/gsl>.
- [22] E. Anderson et al., *LAPACK Users' Guide* (Society for Industrial and Applied Mathematics, 1999).
- [23] N. J. A. Sloane, *On-Line Encyclopedia of Integer Sequences*, <http://oeis.org/A000088>.